A procedure to estimate cutoff wall transport properties from monitoring wells

A procedure to estimate cutoff wall transport properties from monitoring wells

Giulia Guida *[1], Guido Musso[2], Gianluigi Sanetti[3], Claudio di Prisco[1], and Gabriele Della Vecchia[1]

[1]Politecnico di Milano, Dipartimento di Ingegneria Civile e Ambientale (DICA)

[2]Politecnico di Torino, Dipartimento di Ingegneria Strutturale, Edile e Geotecnica (DISEG)

[3]Italian Ministry for the Economic Development (DGS-UNMIG)

Abstract

Owing to their capability in limiting the transport of pollutants in the subsoil, cutoff walls are popular solutions for the confinement of contaminants. These barriers are often made of soil-bentonite or cement-bentonite mixture, which are characterized by low hydraulic conductivity, low hydrodynamic dispersion and long-term durability. However, the aggressive chemical environment to which these walls are subjected might negatively impact on their performance. Assessment of their performance with time is thus a crucial issue in wall design. The use of dedicated monitoring wells, cast in place inside the wall during construction when the bentonitic mixture is still fluid, can be particularly suitable for both intercepting and detecting the fluids flowing through the barrier. In this research, the results of a numerical study aimed at providing a methodology to estimate the transport properties of the backfill material at the site scale are presented. The methodologies relies on abaci and only requires the flow and concentration within a monitoring well inside the barrier to be known.

*giulia.guida@polimi.it

1 Introduction

In both geotechnical and geoenvironmental applications, cutoff walls are aimed at controlling groundwater flow and pollutant migration, providing at the same time a negligible long-term environmental impact. Initially, cutoff walls were used for hydraulic applications, *e.g.* to prevent piping in dams (Cermak *et al.*, 2012) and groundwater flow into excavations (Opdyke and Evans, 2005). Subsequently, they started being applied also to remediation and securing of polluted areas, *e.g.* waste disposal and contaminant insulation (Jefferis, 1981; Rowe, 2005). For both applications, low hydraulic conductivity and long-term durability are required. These requirements are fulfilled by constructing the barriers by using either soil-bentonite or cement-bentonite mixtures (Ryan, 1985; Evans, 1993; Rumer and Mitchell, 1995). The site efficiency of the barrier system, however, depends not only on the properties of the mixture, but also on many other factors, such as the construction method, the presence of impurities and defects, and chemical interactions between the mixture and the pollutant (Joshi *et al.*, 2009).

The construction methods for soil- or cement-bentonite slurry trench cutoff walls are well-established (Ryan, 1987; Evans, 1993). A narrow (typically 0.5 to 1 m wide) slurry filled trench is first excavated in the subsurface. The slurry ($\sim 5\%$ bentonite and $\sim 95\%$ water) is employed to maintain trench stability as the excavation proceeds downward from the ground surface. For soil-bentonite filling, as the excavation proceeds longitudinally, the trench is backfilled by displacing the slurry with a mixture of soil, bentonite-water slurry, and occasionally dry bentonite (Malusis and McKeehan, 2013). The soil used in the backfill may be soil excavated from the trench, borrow soil imported from off-site, or a mixture of both, depending upon grain size characteristics, the presence/absence of contamination and hydraulic conductivity requirements. For the cement-bentonite mixtures, the slurry incorporated with cementitious binder (usually containing Portland cement but often blended with ground blast furnace slag or pulverised fuel ash) is left to harden in place, *i.e.* without a backfill soil, to form the cutoff wall (Jefferis, 2012). Cement-bentonite may be the backfill choice where strength considerations indicate the need for a material stronger than a soil-bentonite backfill (Jefferis, 1981).

Specifications in the U.K. (Institution of Civil Engineers, 1999) require the hydraulic conductivity of the backfill material at 90 days to be less than 10^{-9} m/s for at least 80% of laboratory

cured samples. However, the hydraulic conductivity of the barrier in the field depends on many factors which, in general, cause it to be higher than the one measured in the laboratory (Barvenik and Ayres, 1987; Ryan, 1987; Trivedi *et al.*, 1992; Evans, 1993, 1994; Manassero, 1994; Sanetti, 1998; Filz *et al.*, 2001; Britton *et al.*, 2005; Sanetti, 2006). The complexity and the variability of these factors –*i.e.* as defects and fractures related to the construction, to the oscillation of the groundwater level and interaction with the atmosphere, chemical changes in the material fabric due to the aggressive ground conditions– imply that an *a priori* estimate of the *in situ* hydraulic conductivity is not possible, even if laboratory test results are available (Fratalocchi *et al.*, 2006; Du *et al.*, 2015; Evans *et al.*, 2017).

In situ measurements and monitoring of barrier properties are, therefore, an important issue, and the field hydraulic barrier performance should always be verified after installation. Due to the difficulties related to the collection of high-quality solid core samples from the constructed walls, Manassero (1994) and Takai *et al.* (2016) proposed a site evaluation of the hydraulic conductivity of the backfill material by means of cone penetration (CPTU) testing. The techniques adopted, however, may induce a permanent damage to the barrier, due to the penetration of the device into the solid backfill. Among non-invasive techniques, the solution generally used consists in excavating monitoring wells outside the diaphragm (Sanetti, 2000), in the area to be protected from pollution. However, in this case, the contaminant is detected only after migration through the barrier. An alternative solution has been introduced by Grisolia and Napoleoni (1997), who performed *in situ* constant-head hydraulic conductivity tests via a piezometer installed in the barrier when the trench mixture is still in the slurry state. Accordingly, Sanetti (1998) proposed the installation of monitoring/measuring wells in the liquid slurry, avoiding the perforation of the wall and the related damage, and allowing to test the performance of a large volume of the system. The goal of these wells is to collect the fluid passing through the barrier before the leachate contaminates the surrounding environment, allowing an early identification of contaminants and an assessment of the efficiency of the barrier. Monitoring wells can also be used to check undesired permeability changes and an early identification of transport species (Trivedi *et al.*, 1992; Fratalocchi *et al.*, 2006).

This paper explores a systematic numerical analysis of the process of contaminant transport throughout cutoff walls that contain monitoring wells. In particular, a procedure to exploit

measurements performed in the wells to estimate the hydro-chemical properties of the barrier is presented. The procedure is synthesized in terms of dimensionless quantities, facilitating different geometrical configurations of both barrier and well, and different hydraulic conditions at the inlet and outlet of the wall.

2 Cut-off wall with monitoring wells: geometrical scheme

In this study, the cutoff wall is assumed to be installed to insulate a polluted area from a freshwater aquifer (Figure 1). The combination of the wall and the contaminated area are considered to be large relative to the wall thickness, such that end effects can be disregarded along the longitudinal direction of the wall. The water level in the polluted area was considered to be either higher (worst case scenario, such as reported in Figure 1), or lower than the aquifer hydraulic head, providing diffusive and advective fluxes in either the same (as is shown in Figure 1) or opposite direction.

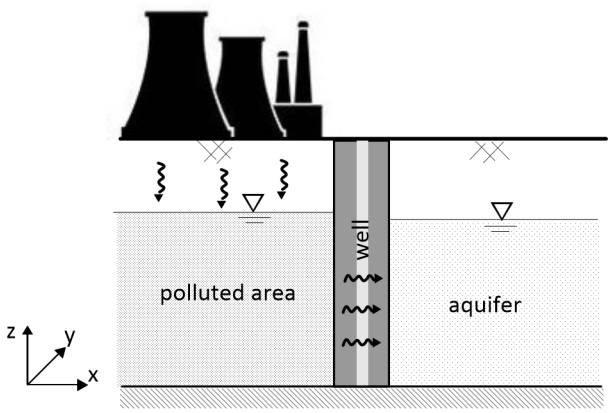

Figure 1: Schematic view of the cutoff wall, with a monitoring well.

The simulation of contaminant transport and water flow through a barrier without wells is generally performed under one-dimensional conditions, since (i) the barrier length is much larger than its thickness, l, and (ii) the flux direction across the barrier, according to the *Dupuit* assumption, is assumed to be horizontal. A three-dimensional scheme for the barrier with wells is shown in Figure 2. In the presence of wells of diameter d, transversally centered and spaced a distance s apart, the flow of water can be still treated as horizontal but two-dimensional in

the horizontal plane. Nonetheless, by assuming homogeneity of the barrier, the symmetry of the problem allows to study just a segment of the wall centered in the wells, s long and l thick (dark area in Figure 2).

From the geometrical point of view, the system can thus be described, for a given thickness l, by just two geometrical dimensionless variables: (i) the normalized diameter d/l of the well, and (ii) the normalized spacing s/l. In the numerical study, different geometrical configurations of the system were considered.

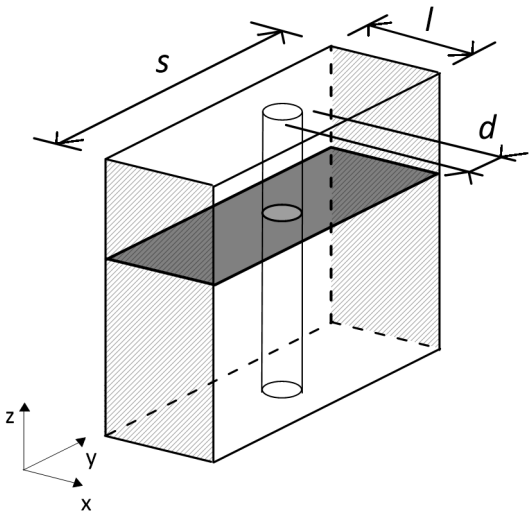

Figure 2: Three-dimensional scheme of the cutoff wall with monitoring well.

3 Field equations for dilute contaminant transport across the barrier

3.1 Modelling assumptions

The flux of a dissolved contaminant in a saturated cutoff wall is considered. Accordingly, the solution of two field equations is required, namely the water mass balance equation and the contaminant mass balance equation. The model was kept as simple as possible, while trying to find a compromise between reproduction of all the relevant physical processes, the need for the inverse problem to be well-posed, and robustness of application in engineering design. Accordingly, the backfill material was assumed homogeneous and isotropic in terms of transport properties, *e.g.* hydraulic conductivity and hydrodynamic dispersion. Progressive enhancement

(or otherwise, decay) of the hydraulic properties of the backfill were not considered. The evidence exists that the permeability of some mixtures continues to decrease over long times, *e.g.* the permeability of the blast furnace slag cement with an activated Na-bentonite tested by Fratalocchi *et al.* (2006) reached a stable value only after 300 days in tap water. However, introducing such time dependency in the numerical simulations would not significantly change the contaminant breakthrough time, as showed in the sensitivity analysis presented in Appendix 1. Also, any physico-chemical interaction between the constituents of the barriers and the contaminated ground water were not considered. Overall, the present methodology aims to provide a tool for a quick and proper evaluation of the current transport parameters at the field scale. Both anomalously high values and values that increase with time are key indicators of malfunctions of the barrier.

3.2 Water mass balance equation

Water flow across the barrier is governed by the Darcy law (Equation 1):

$$\mathbf{v} = -K\nabla h, \tag{1}$$

where $\mathbf{v}$ il the water velocity field in the domain, K is the hydraulic conductivity and ∇h is the gradient of the hydraulic head. Under the assumption of constant water density, negligible porosity changes, isotropic and homogeneous hydraulic conductivity, the two-dimensional mass balance is expressed by the Laplace equation:

$$\nabla^2 h = \frac{\partial^2 h}{\partial x^2} + \frac{\partial^2 h}{\partial y^2} = 0, \tag{2}$$

where x and y are the horizontal reference coordinates.

The imposed hydraulic boundary conditions adopted are illustrated in Figure 3a. A constant hydraulic head h_{in} is applied at the inlet boundary (in contact with the polluted area), while a constant hydraulic head h_{out} is applied at the outlet boundary (in contact with the aquifer). These head values are set accordingly to the *in situ* water table levels. Lateral flow is not permitted ($\partial h/\partial y = 0$). At the well boundaries, a hydraulic head h_{well} is imposed. All the results are presented in terms of the non-dimensional quantity h^*_{well}, defined as follow:

$$h^*_{well} = \frac{h_{well} - h_{out}}{h_{in} - h_{out}}. \tag{3}$$

If $h^*_{well} = 0$ the hydraulic head in the well coincides with that at the outlet, $h_{well} = h_{out}$. If, in contrast, $h^*_{well} = 1$, the hydraulic head in the well coincides with that at the inlet, $h_{well} = h_{in}$.

3.3 Contaminant mass balance equations

The flux $\mathbf{j}$ represents the quantity of contaminant passing through a unitary area of porous medium in a time increment, and is expressed as:

$$\mathbf{j} = c\mathbf{v} - D\nabla c. \tag{4}$$

The first term represents the advective contribution, depending on the hydraulic gradient through *Darcy* velocity $\mathbf{v}$ (Equation 1). The second term represents the diffusive contribution, related to the gradient of contaminant concentration via the hydrodynamic dispersion D, accounting for both molecular diffusion and mechanical dispersion (Shackelford, 1990; Della Vecchia and Musso, 2016).

The transport of a dissolved contaminant in water is governed by the contaminant mass balance equation. Assuming negligible changes in porosity and complete saturation, the contaminant mass balance is expressed by the advection-diffusion equation (*e.g.* Rowe *et al.* 1995; Bear 2013), according to which the variation in contaminant concentration c with time is related to the divergence of the contaminant mass flux $\mathbf{j}$:

$$R\frac{\partial c}{\partial t} + \nabla \cdot \mathbf{j} = 0, \tag{5}$$

where R is the retardation factor. If no adsorption of contaminant occurs, R is equal to 1. For solutes subject to reversible, linear and instantaneous (equilibrium) adsorption reactions during diffusive transport (Smith and Jaffe, 1994), R is greater than 1, representing a retard action on the contaminant migration.

The barrier is assumed to be initially free of contaminant, or:

$$c(x, y, t = 0) = 0. \tag{6}$$

The choice of the appropriate boundary conditions for contaminant flux into barriers is not straightforward (Rabideau and Khandelwal, 1998; Prince *et al.*, 2000; Li *et al.*, 2017). However, it could have a strong impact on numerical results, especially when advection dominates diffusion, *i.e.* for values of the *Peclet* number $Pe = |\mathbf{v}|l/D \geq 20$ (Van Genuchten and Parker, 1984).

Figure 3b shows the chemical boundary conditions adopted for the barrier in accordance to Brenner (1961) suggestion:

- at the inlet boundary, a *Robin* boundary condition is imposed, in order to guarantee contaminant mass conservation between the polluted area and the cutoff wall (Van Genuchten and Parker, 1984):

$$\mathbf{v}c - D\nabla c = \mathbf{v}c_0, \tag{7}$$

  where c_0 is the contaminant concentration in the polluted area;

- at the outlet boundary, according to Brenner (1961), solute concentration is assumed to be continuous between the barrier and the aquifer: $\partial c/\partial x = 0$. Following the observation by Rabideau and Khandelwal (1998), the case of a perfectly flushing boundary condition was also considered, and it did not have significant impact on the methodology results (see Appendix 2);

- across the lateral sides of the domain, symmetry requires the imposition of no flux conditions, *i.e.* $\partial c/\partial y = 0$.

Finally, a proper boundary condition is needed for the contaminant at the well boundary Γ_d. This condition was chosen by imposing the mass balances to the well system. As for the water, in order to maintain a constant hydraulic head in the well (Section 3.2), the water flow entering the well q^{in}_{well} must be equal to the water flow pumped outside the well q^{out}_{well}:

$$q^{in}_{well} = q^{out}_{well} = q_{well}, \tag{8}$$

where $q_{well} = v_{av}\pi d$, being v_{av} the average Darcy velocity of water across well boundary Γ_d whose normal unit vector is $\mathbf{n}$: $v_{av} = 1/(\pi d)\int_{\Gamma_d}(\mathbf{v}\cdot\mathbf{n})\mathrm{d}\Gamma$. Solute mass balance implies that the variation in contaminant mass inside the well is ruled by the difference between the inlet (j^{in}_{well}) and the outlet ($j^{out}_{well} = cv_{av}$) average contaminant flux:

$$V_{well}\frac{\partial c}{\partial t} = S_{well}\left(j^{in}_{well} - cv_{av}\right), \tag{9}$$

where $V_{well} = \pi d^2/4$ is the volume of the well per unit depth, and $S_{well} = \pi d$ is the lateral surface of the well per unit depth. Note that q_{well} is greater than zero only when $h^*_{well} < 0.5$ (Scelsi *et al.*, 2019). Further, although low hydraulic conductivity barriers ($K \sim 10^{-9} m/s$) are considered, a measurable quantity of the outflow can be obtained in reasonable range of time (see the Examples on Sect.5.3).

The contaminant mass balance differential equation (Eq. 9) rules the variation with time of the concentration within the well. This concentration is then imposed at the boundary between the well and the barrier, leading to a concentration inside the well that is updated at every time step.

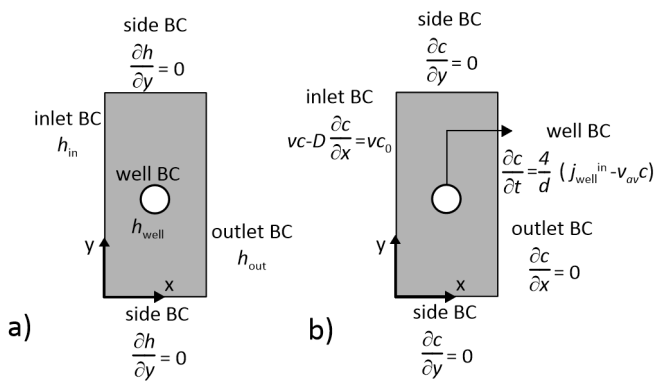

Figure 3: a) Boundary conditions for the water mass balance equation. b) Boundary conditions for the solute mass balance equation.

4 Scenarios analyzed in the numerical simulations

The system of Equations 2 and 5 was solved numerically by employing the Finite Element Method using Comsol Multiphysics.

Two hydraulic scenarios (Britton *et al.*, 2005; Neville and Andrews, 2006) were considered (see Figure 4):

- Hydraulic Scenario 1 (HS1, Figure 4a): the hydraulic head in the polluted area is greater than at the outlet, and $\Delta h = h_{out} - h_{in} < 0$. In this scenario, the boundary conditions are such that both the advective and the diffusive fluxes are in the same direction in the absence of the well, *i.e.* from the contaminated area to the aquifer. The normalized hydraulic head inside the well h^*_{well} should be lesser than 0.5, in order to avoid water flow from the well to the aquifer (Scelsi *et al.*, 2019).

- Hydraulic Scenario 2 (HS2, Figure 4b): the hydraulic head in the polluted area is kept lower than the one in the aquifer, and $\Delta h = h_{out} - h_{in} > 0$. The boundary conditions are such that the advective and the diffusive fluxes are in opposite directions. This scenario reduces the contaminant flux towards the aquifer.

HS1 is the most unfavourable for the containment of the contaminant, because both advection and diffusion drive the pollutant toward the aquifer. In HS2, advection and diffusion may partially balance and depending on the Peclet number one dominates over the other.

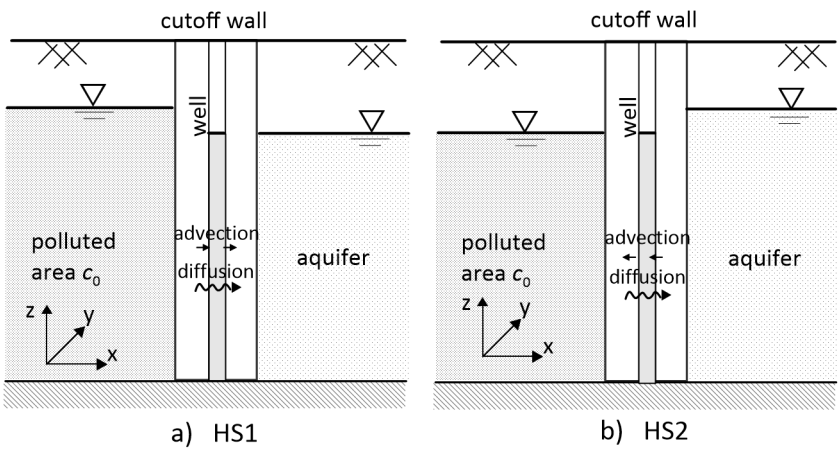

Figure 4: Scheme of the different hydraulic scenarios analyzed: a) Hydraulic Scenario 1 (HS1) with $h^*_{well} = 1$ and b) Hydraulic Scenario 2 (HS2) with $h^*_{well} = 1$.

5 Exploiting monitoring wells to estimate in situ transport properties

Scelsi *et al.* (2019) proved that, for certain geometrical configurations and boundary conditions, the presence of the wells may contribute to mitigate and retard the contaminant flux through the barrier. For instance, when $h^* \leq 0.5$, water is drained by the well and the transport

of contaminant towards the aquifer is retarded by this drainage. This paper focuses on the information which can be obtained exploiting the wells for monitoring purposes. The most evident application is the detection of the presence of contaminants crossing the barrier, by analysing the chemical composition of the flowing water. The detection of a contaminant halfway towards the aquifer –*i.e.* many years in advance– is certainly beneficial. However, the paper proposes a further use of monitoring wells: if the water discharge into the wells is measured and the water chemistry is analyzed, this information can be exploited in order to estimate the *in situ* transport properties of the barrier via back analysis. In particular, water flow into the well allows for the hydraulic conductivity to be estimated, while the breakthrough curves of contaminant flux into the well can be used to obtain the hydrodynamic dispersion and the retardation factor. Once determined via the measurements performed at the site, the current values of hydraulic conductivity and hydrodynamic dispersion may be used to update the predictions of the barrier performance.

5.1 Hydraulic conductivity estimate

The water flow entering into the well q_{well} depends on the difference between the hydraulic head in the well and the hydraulic heads at the inlet and the outlet, *i.e.* on the normalized hydraulic head in the well h^*_{well}. Figure 5 shows an example of the role of h^*_{well} on the normalized hydraulic head distribution $h^*(x, y)$ inside the barrier and on the flow lines. $h^*(x, y)$ was defined as:

$$h^*(x, y) = \frac{h(x, y) - h_{out}}{h_{in} - h_{out}}. \tag{10}$$

The two-dimensional flow path induced by the well is evident for $h^*_{well} = 0$, (Figure 5a). For $h^*_{well} = 0.4$, the flow path is less affected by the presence of the well. For given hydraulic boundary conditions and a given geometrical configuration of the wells, then the water flow entering into the well q_{well} can be directly linked to the hydraulic conductivity K of the barrier. To this aim, several FEM numerical analyses solving the stationary water mass balance equation were performed, with the aim of creating the non-dimensional plots of Figure 6. These abaci provide the evolution of the non-dimensional group $K|\Delta h|/q_{well}$ with the non-dimensional well spacing s/l for different well diameters d/l and well normalized hydraulic heads h^*_{well}. Only

cases with water flow entering into the well ($q_{well} > 0$) are exploited. This means that for HS1, $h^*_{well} = h^*_{HS1} < 0.5$, while for HS2 $h^*_{well} = h^*_{HS2} > 0.5$.

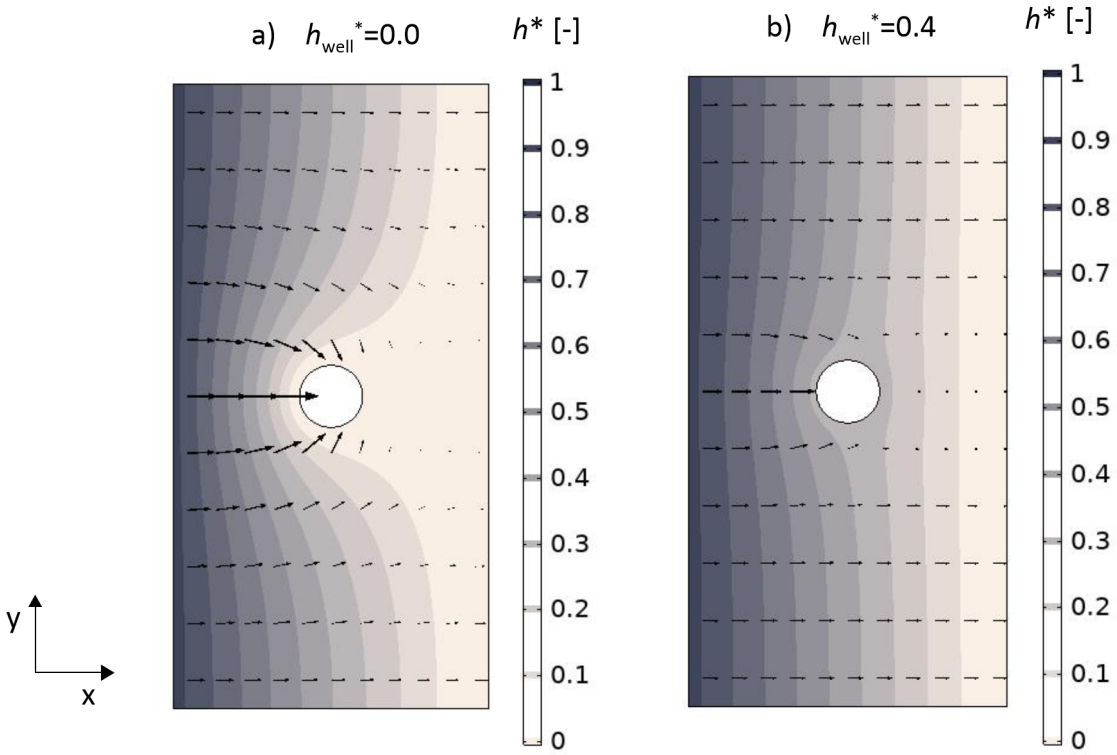

Figure 5: Contour plots of the hydraulic head and water velocity field for two different normalized water heads inside the well: a) $h^*_{well} = 0.0$ and b) $h^*_{well} = 0.4$, for $d/l = 0.2$ and $s/l = 2$.

The procedure to estimate the hydraulic conductivity of the barrier K is:

1. Select the relevant value of the hydraulic head h_{well} and compute the corresponding dimensionless value h^*_{well};
2. Select the relevant value of well spacing s/l and diameter d/l;
3. Obtain from the abacus in Figure 6 the corresponding non-dimensional value of $K|\Delta h|/q_{well}$;
4. Measure *in situ* the water flow in the well q_{well};
5. Estimate K by multiplying the non-dimensional ratio by $q_{well}/|\Delta h|$.

A block diagram summarizing the logical steps of the procedure to estimate K is reported in Figure 7. From Figure 6, as s/l increases, the corresponding variation in $K|\Delta h|/q_{well}$ becomes negligible. This is related to the fact that, for values s/l larger that 2, the discharge q_{well} starts to be independent from well spacing, due to the finite area of influence of the well.

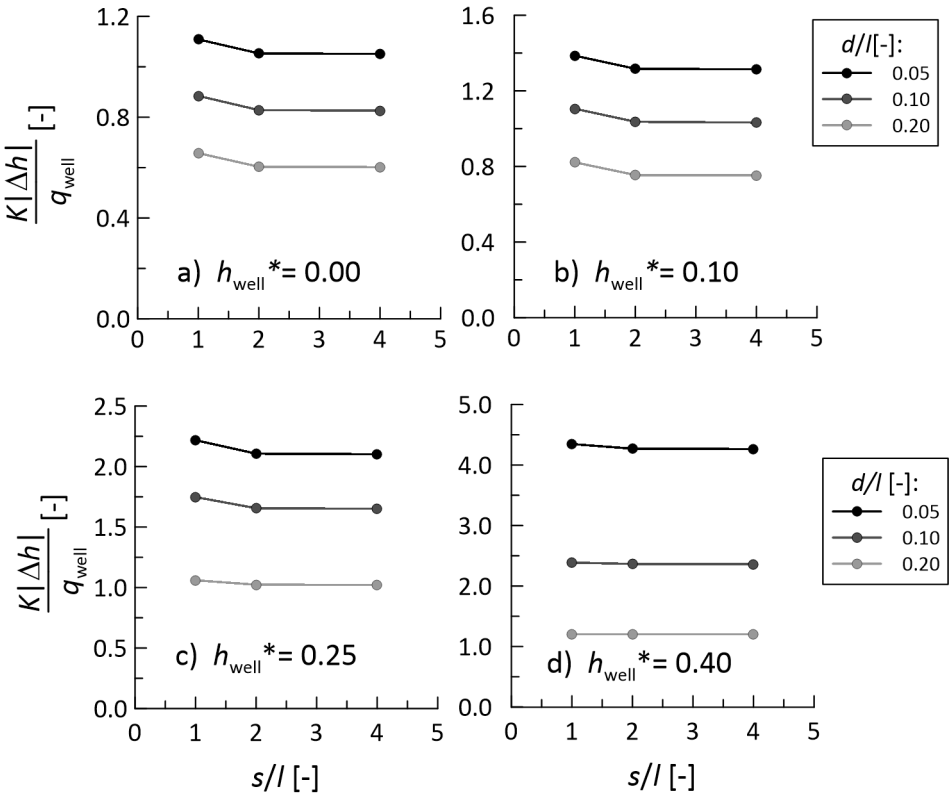

Figure 6: Non-dimensional abaci to determine the *in situ* hydraulic conductivity of the barrier.

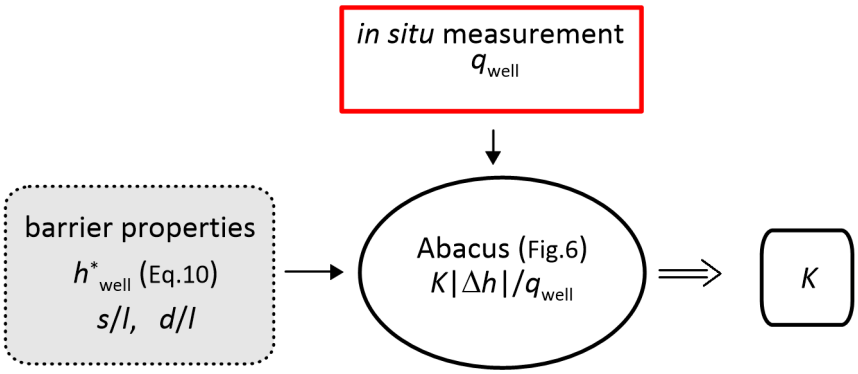

Figure 7: Procedure for the assessment of K.

5.2 Hydrodynamic dispersion and retardation factor estimate

Once the hydraulic conductivity is known, the contaminant concentration measured within the well can be exploited to estimate the hydrodynamic dispersion and the retardation factor of the barrier.

Parametric analyses were performed to identify the effects of the hydrodynamic dispersion D and retardation factor R on concentration breakthrough curves in the well, accounting for both hydraulic scenarios HS1 and HS2. The results are summarized in Figure 8, where just non-dimensional variables were used, namely

- The normalized concentration c/c_0, *i.e.* the ratio of current concentration with respect to the constant concentration of the polluted area;
- The Peclet number $Pe = K|\Delta h|/D$, describing the relative role of advection with respect to diffusion, *i.e.* of hydraulic conductivity with respect to the hydrodynamic dispersion;
- The non-dimensional time $T = K|\Delta h|t/l^2$.

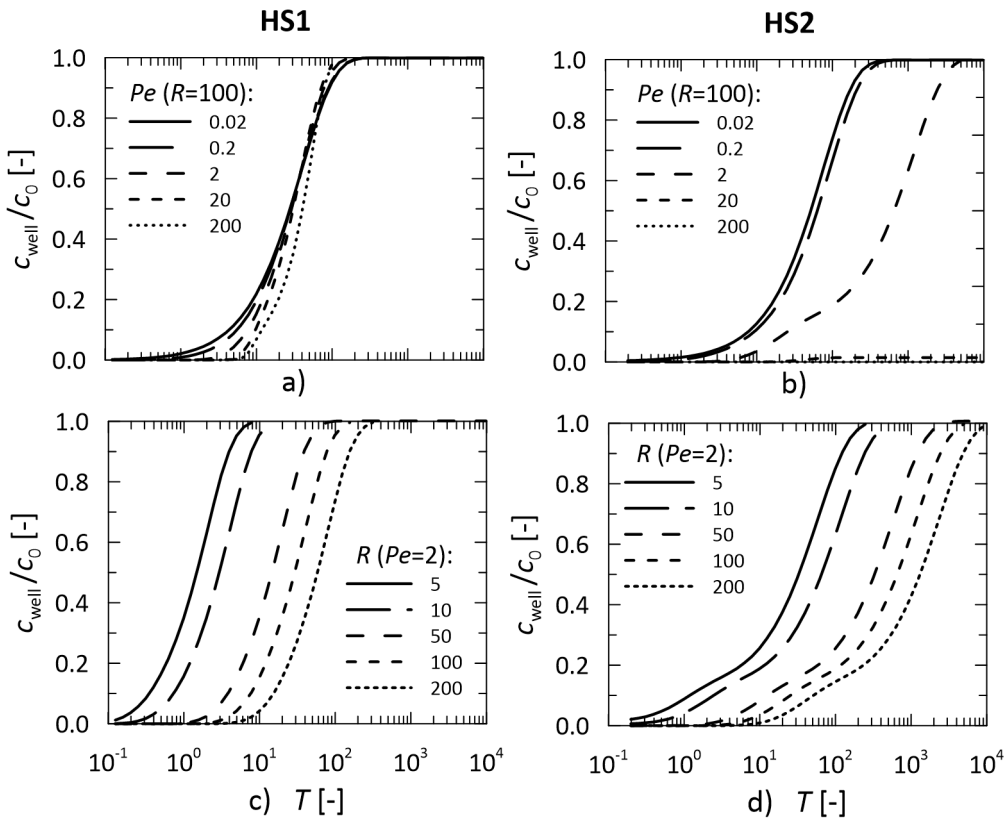

Figure 8: Concentration evolution into the well for scenarios HS1 and HS2, by varying a,b) the Peclet number Pe and c,d) the retardation factor R. $h^*_{well} = 0$, $s/l = 2$ and $d/l = 0.2$ were assumed in all the simulations.

In Figure 8a, corresponding to hydraulic scenario HS1 and $h^*_{well} = 0$, the arrival of the contaminant at the well, in terms of non-dimensional time, increases for increasing Peclet number, as well as the slope of the breakthrough curve in the log time scale. The effect of an increase in the retardation factor R (Figures 8c) is to shift the breakthrough curve toward longer times while maintaining the same shape. This observation is also valid for hydraulic scenario HS2 (Figure 8d). As for the role of the Peclet number in scenario HS2 (Figure 8b), it is worth noting that the contaminant does not get the well when advection dominates diffusion, *i.e.* for $Pe \geq 20$. The role of advection in modifying the shape of breakthrough curves of contaminant in the well is however already evident for $Pe = 1$.

In order to estimate the hydrodynamic dispersion, the rate of concentration change in the well evaluated in a log time scale, being almost independent on the retardation factor, appears as an appropriate variable (to measure in site). For practical purposes, the slope θ can thus be defined as:

$$\theta = \frac{1}{c_0} \frac{c_{well}(t_1) - c_{well}(t_0)}{\log\left(\frac{t_1}{t_0}\right)}, \tag{11}$$

where t_0 and t_1 are the times corresponding to a given value of the non-dimensional concentration ratio c_{well}/c_0: *i.e.* equal to 1% and 5%, respectively.

Figure 9 and 10 report abaci of the relation between θ and D for different spacing s/l, diameters d/l and normalized hydraulic head inside the well h^*_{well} for both hydraulic scenarios. As expected, for hydraulic scenario HS1 (Figure 9), a lower value of D corresponds in general to larger values of θ. When the transport mechanism is dominated by the hydrodynamic dispersion (*i.e.* $D/(K|\Delta h|) > 5$, corresponding to $Pe < 0.2$), the curves are the same regardless of the value of h^*_{well}. When the dominant transport mechanism is the advection, the value h^*_{well} becomes more relevant. For Scenario HS2, as shown in Figure 10, only Peclet numbers lower than 1 are considered (*i.e.* $D/(K|\Delta h|) > 1$). For larger Peclet numbers, the advective flux (directed from the outlet to the inlet) limits the diffusive flux of contaminant (directed from the inlet to the outlet), leading to a reduction in θ with increasing $D/(K|\Delta h|)$ up to invalidate the parameter estimate procedure. The role of spacing s/l in the abaci of Figure 9 and 10 is limited, with a slight tendency to provide an increase in slope θ for increasing s/l, especially for low D. The influence of diameter d/l is more relevant, because it changes the distance between barrier boundaries and the well. In particular, for HS1, the larger the well diameter d/l, the smaller the slope θ (Figure 9). In contrast, an increase in d/l implies an increase in θ for HS2 (Figure 8).

Figure 11 and 12 report abaci of the relation between the dimensionless ratio of $D/(K|\Delta h|)$ and the non-dimensional group $Rl^2/(t_0 K|\Delta h|)$. Also in this case, different well configurations in terms of spacing s/l, diameter d/l and well normalized hydraulic head h^*_{well} are considered. Given the time of contaminant detection t_0, the retardation factor decreases with D, and stabilizes for $D/(K|\Delta h|) < 10^{-1}$. The spacing between wells does affect significantly the trend for

HS1, as is shown in Figure 9, but is more relevant for HS2.

The procedure for assessing the chemical transport properties of the barrier, by the use of the abaci of Figs. 9–12 as follow is illustrated in Fig.13:

1. monitor the time evolution of contaminant concentration inside the well and determine the time t_0, corresponding to a non-dimensional contaminant concentration ratio $c(t_0)/c_0 =$

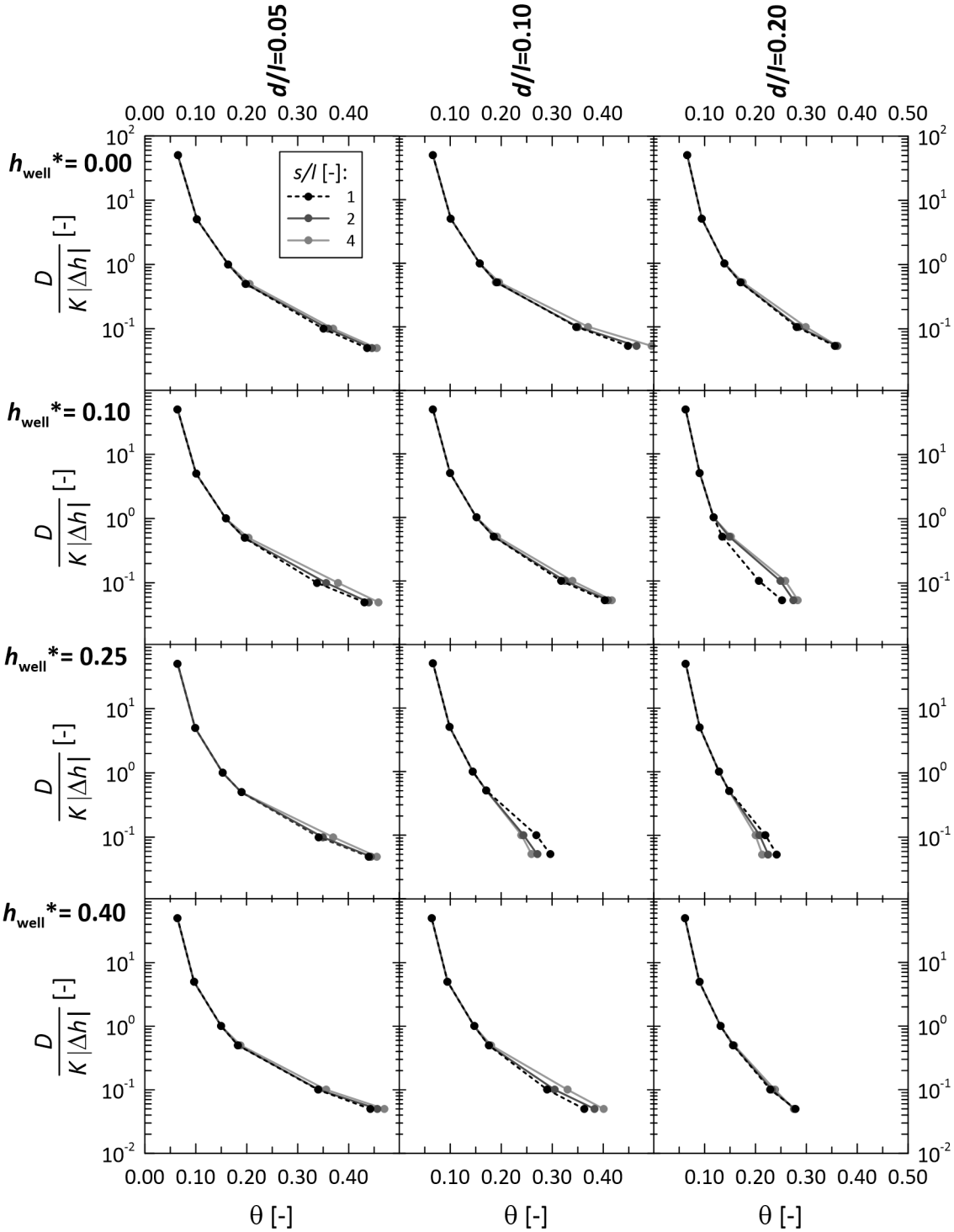

Figure 9: Abacus for the estimation of the hydrodynamic dispersion D as a function of d/l, s/l and h^*_{well} for a hydraulic regime HS1.

1%;

2. determine the time t_1, corresponding to a non-dimensional contaminant concentration ratio $c(t_1)/c_0 = 5\%$;

3. calculate by means of Eq. 11 the value of θ;

4. given the well spacing, diameter and hydraulic head, estimate from Figure 9 or 10 the

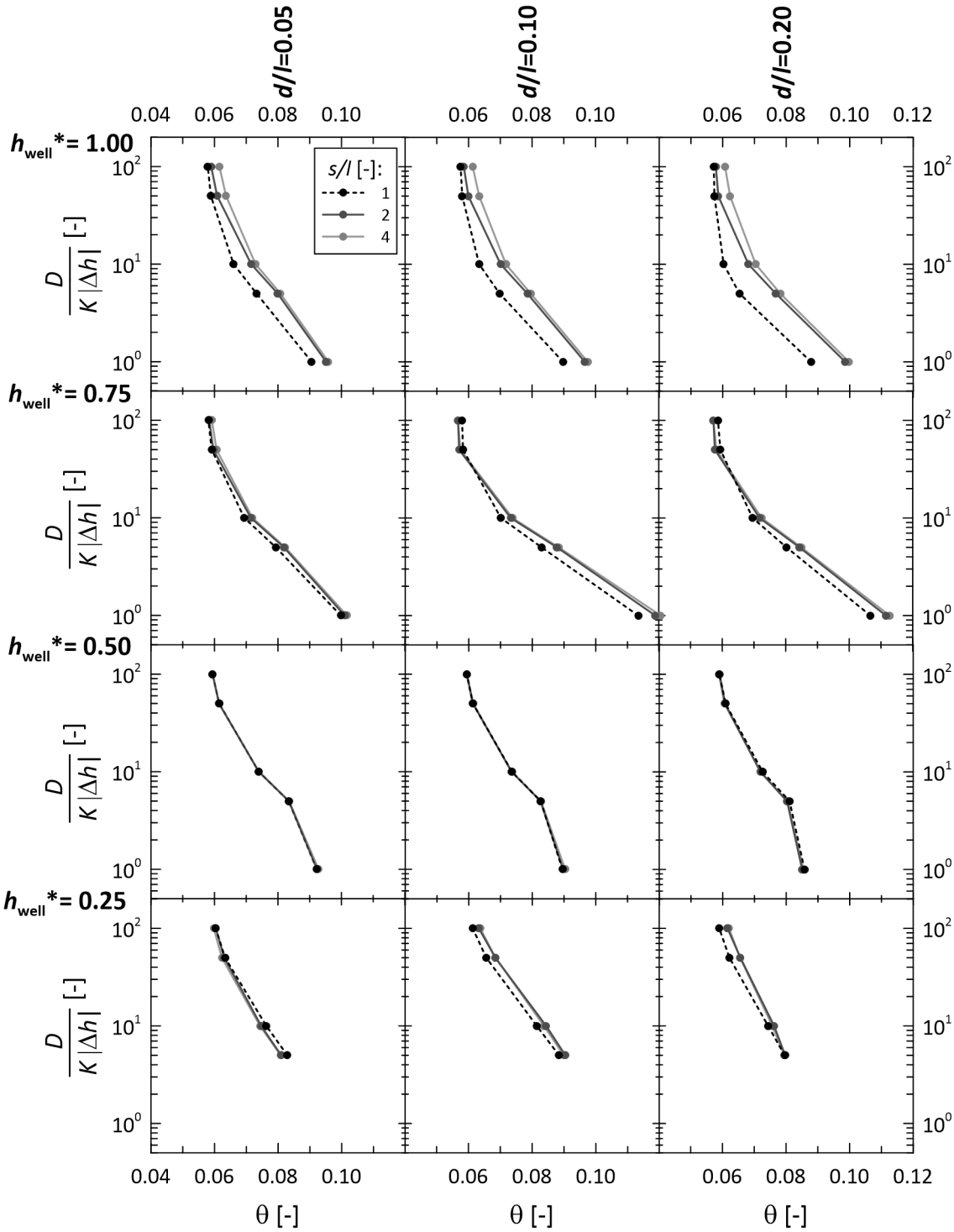

Figure 10: Abacus for the estimation of the hydrodynamic dispersion D as a function of d/l, s/l and h^*_{well} for a hydraulic regime HS2.

value of the non-dimensional group $D/(K|\Delta h|)$;

5. after determining K (from the procedure described in Sect. 5.1) and Δh, estimate the hydrodynamic dispersion, D;

6. with D, determine the value of $D/(K|\Delta h|)$ and use Figure 11 or 12 to estimate the non-

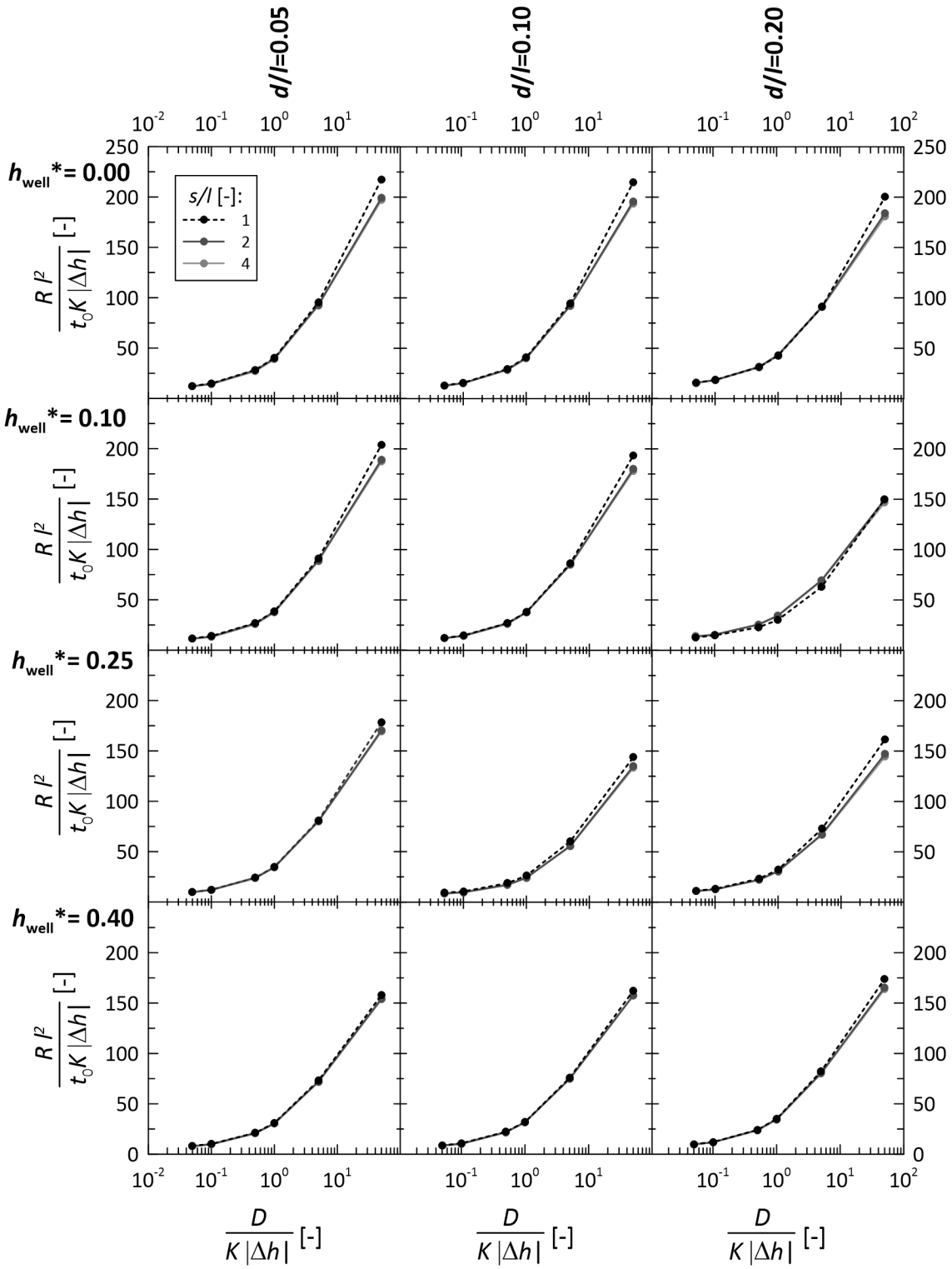

Figure 11: Abacus for the assessment of R as a function of d/l, s/l and h^*_{well} (hydraulic regime HS1).

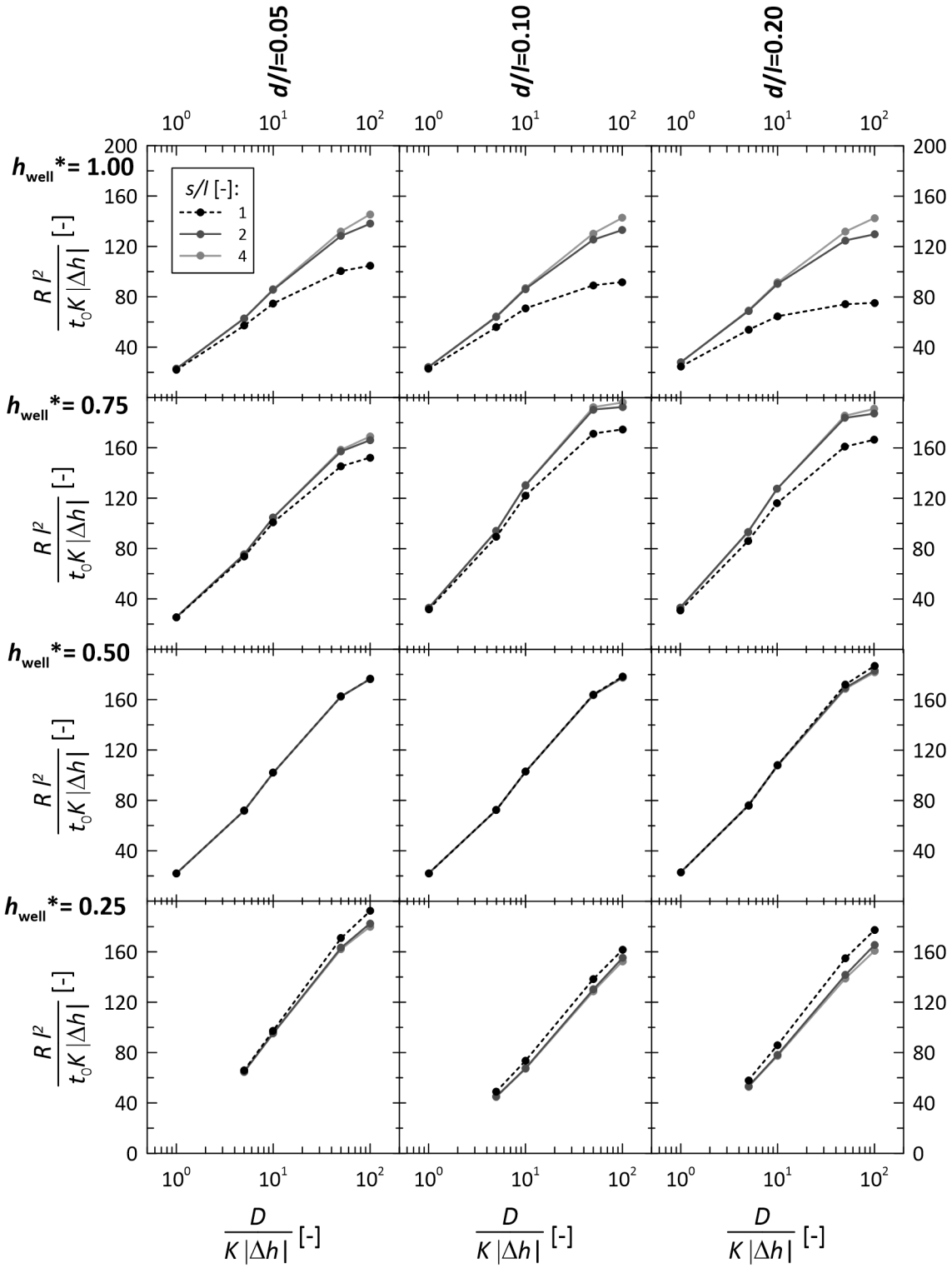

Figure 12: Abacus for the assessment of R as a function of d/l, s/l and h^*_{well} (hydraulic regime HS2).

dimensional group $Rl^2/(t_0K|\Delta h|)$;

7. with the known t_0, estimate the retardation factor as $R = \dfrac{t_0K|\Delta h|}{l^2}$.

The same non-dimensional results reported in the abaci of Figures 9-12 apply also for the flushing zero concentration boundary condition of no contaminant in the aquifers (see Appendix 2 for the detailed explanation).

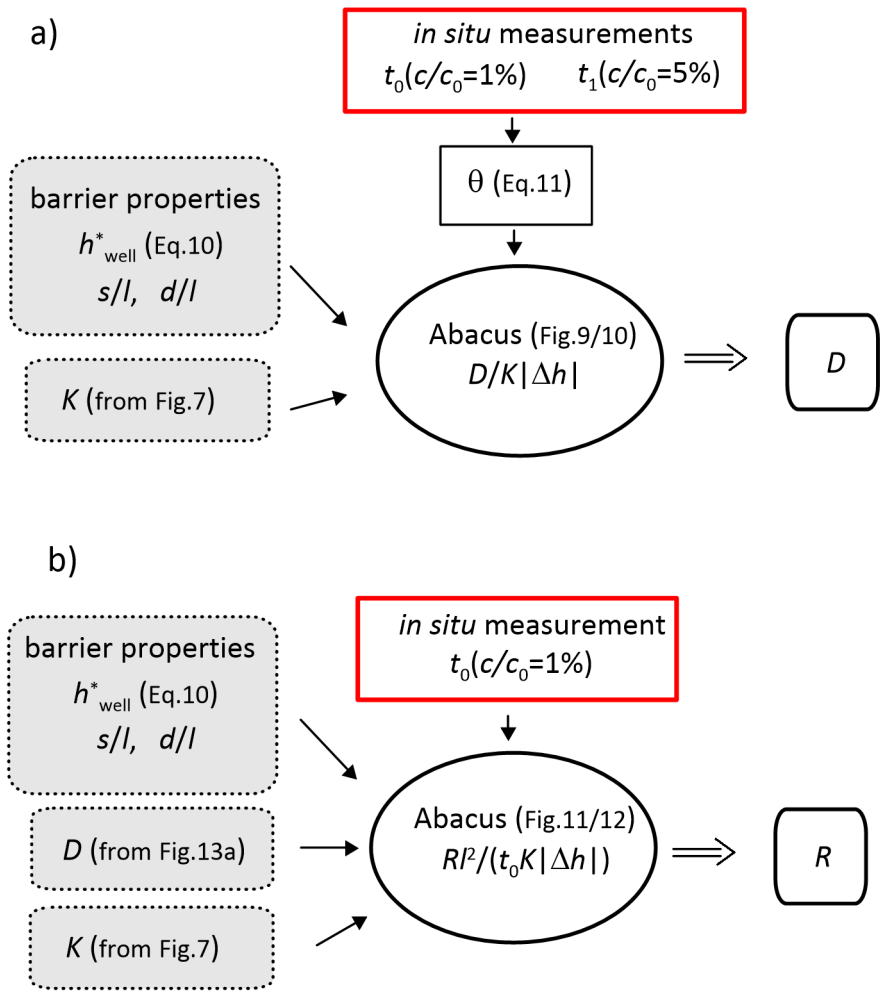

Figure 13: Procedure for the assessment of a) D and b) R.

5.3 Examples of application of the procedure

In this section, two numerical examples applied to a cutoff wall characterised by different hydraulic scenarios (HS1 and HS2) are illustrated. The geometrical properties and boundary conditions are given in Table 1.

Table 1: Geometry and material parameters used in the numerical examples (Scelsi *et al.*, 2019).

Wall thickness	l	0.4	m
Well diameter	d	8	cm
Well spacing	s	0.8	m
Inlet hydraulic head	h_{in} (HS1/HS2)	3.0/2.0	m
Outlet hydraulic head	h_{out} (HS1/HS2)	2.0/3.0	m
Well hydraulic head	h_{well}	2.0	m
Concentration in the polluted area	c_0	10	mol/m^3

Assume that for an hydraulic scenario HS1 a steady-state discharge of q_{well} ~15.0 cm^2/d

per unit depth is measured *in situ* . Since the level of hydraulic head in the monitoring well is maintained constant, a pump will remove the exceeding volume of water. Measuring the volume lifted over the range of time, is possible to extrapolate a value of the water discharge q_{well}.

The procedure proposed in Figure 7 can be applied to estimate the hydraulic conductivity K:

1. once known the hydraulic head in the well and the hydraulic heads at the inlet and at the outlet (Tab.1), the normalized water head in the well $h^*_{well} = 0$ is calculated according to Eq. 3;
2. the dimensionless spacing $s/l = 2$ and diameter $d/l = 0.20$ of the well are calculated from the relevant values of barrier geometrical properties (Tab. 1);
3. by entering in the abacus of Figure 6a with $d/l = 0.20$ and $s/l = 2$, a value of the dimensionless ratio $\frac{K|\Delta h|}{q_{well}} \sim 0.6$ is obtained;
4. and the hydraulic conductivity of the barrier is $K = 0.6\frac{q_{well}}{|h_{in}-h_{out}|} \sim 10^{-8}$ m/s.

Monitoring the value of hydraulic conductivity is thus possible and economical. This would allow evaluating with continuity the hydraulic performance of the barrier. If it changes with time, some process affecting the properties of barrier material is likely to be ongoing, *e.g.* due to chemo-mechanical interaction, and the engineers can take it as an alert to proceed with other interventions.

In the case of scenario HS1, the diffusive and advective fluxes combined and the condition is more critical the higher the hydraulic conductivity of the wall. However, foreseeing the time required for the contaminant to reach the aquifer requires the hydrodynamic dispersion and the retardation factor of the barrier, that can be evaluated by following the procedure described in Section 5.2. The time needed for the contaminant to cross the wall is generally considered of the order of tens of years (Manassero and Shackelford, 1994), thus the shorter the time needed to estimate backfill parameters, the longer the time available to update predictions and to implement maintenance operations. Assuming that, after a time $t_0 = 3$ years a concentration $c_{well} = 0.1$ mol/m^3 (corresponding to $0.01c_0$) is measured, while a concentration $c_{well} = 0.5$ mol/m^3 (corresponding to $0.05c_0$) is measured after $t_1 = 5$ years, the application of the procedure depicted in Figure 13 is as follow:

1. slope $\theta \sim 0.18$ is evaluated (from Eq.11);
2. from Figure 9, for $d/l = 0.2$ and $h^*_{well} = 0.0$ (first row, third column), the slope leads to a value of the non-dimensional group $D/(K|\Delta h|) \sim 0.5$;
3. multiplying the non-dimensional group by $K|\Delta h|$, the value of the hydrodynamic dispersion is obtained, $D \sim 5\text{x}10^{-9}$ m^2/s;
4. from Figure 11, in correspondence to the plot of $d/l = 0.20$ and $h^*_{well} = 0.0$ (first row, third column), it is found that when $D/(K|\Delta h|) = 0.5$ the non-dimensional group $Rl^2/(t_0 K|\Delta h|) \sim 30$;
5. by introducing the current values of t_0, K and Δh, the value of the retardation factor is obtained $R \sim 180$.

In this example, the time required to have a complete characterization of material transport properties can be considered equal to 2 yrs ($= t_1 - t_0$), the numerical model could then be run with the transport parameters estimated *in situ* and the time required by the contaminant to cross the barrier updated. However, when the hydraulic scenario is the HS1 with $h^*_{well} < 0.5$, the time required for the contaminant to reach the aquifer, estimated when the average concentration of contaminant at the outlet $c_{out}/c_0 > 5\%$, is lower than if the well was not present (10 yr with well *vs.* 13 without well).

The same procedure is repeated for a case corresponding to hydraulic scenario HS2, in which $h_{in} = 2.0$ m and $h_{out} = 3.0$ m (see Table 1). In this scenario, the water flows towards the polluted area and the contaminant can reach the aquifer only if $D/(K|\Delta h|) > 1$, *i.e.* diffusion dominates over advection.

Although the direction of flow is the opposite, the geometry and type of boundary conditions for the hydraulic problem are the same as in the previous example, thus $K|\Delta h|/q_{well} = 0.60$. By assuming a steady-state discharge $q_{well} \sim 1.5$ cm^2/d, the resulting hydraulic conductivity of the barrier is $K \sim 10^{-9}$ m/s. Assume, then, that a contaminant concentration $c_{well} = 0.1$ mol/m^3 (corresponding to $0.01c_0$) is measured after $t_0 = 7$ years, while a concentration $c_{well} = 0.5$ mol/m^3 (corresponding to $0.05c_0$) is measured after $t_1 = 19$ years. This sequence implies $\theta \sim 0.09$ (from Eq.11) and by using Fig. 10, *i.e.* the plot corresponding to $d/l = 0.2$ and $h^*_{well} = 1.0$ (first row, third column), to a value of the non-dimensional group $D/(K|\Delta h|) \sim 2$

from which the hydrodynamic dispersion $D \sim 2\text{x}10^{-9}$ m^2/s. From Figure 12 with $d/l = 0.20$ and $h^*_{well} = 1.0$ (first row, third column), $Rl^2/(t_0 K|\Delta h|) \sim 55$ which gives $R \sim 60$.

The procedure requires the presence of the contaminant within the well, and for a given set of parameters the migration of the contaminant is retarded when HS2 scenario is of concern. Determination of the transport parameters requires longer times for this scenario (about 12 yrs for the examined example).

Further, contrary to what seen for HS1, the presence of the well retards the arrival of the contaminant to the aquifer in respect to the case of barrier without wells (23 yrs with well *vs.* 18 yrs of the case without well).

6 Conclusions

The site behaviour of cutoff walls is difficult to predict, due to the complexity and the variability of the factors potentially modifying the transport properties of the backfill material. Presence of defects and impurities related to the construction stage, cracks induced by the oscillation of the groundwater level and chemical interactions related to the aggressive groundwater conditions may serve as examples. This situation implies that *in situ* measurements of barrier transport properties is fundamental for reliable predictions about contaminant transport. In this study, the suitability of using monitoring wells cast in place when the backfill material is still in a slurry state is analyzed, with the aim of providing a methodology to estimate the transport properties of the barrier from site measurements. To this aim, several two-dimensional, finite-element numerical simulations were performed, solving the water and contaminant mass balance equations for boundary conditions relevant for cutoff walls and monitoring wells. In particular, two hydraulic scenarios were considered: one corresponding to advection and diffusion both directed from the inlet to the outlet, and the other with advection directed from the aquifer into the contaminated area. Numerical results were then performed in order to develop non-dimensional abaci, as fast and practical tools to estimate barrier transport properties from periodic measurements performed in the monitoring wells, regardless of the type of mixture adopted. In particular, the methodology allows for the determination of the average (field scale) values of the barrier hydraulic conductivity, hydrodynamic dispersion and retardation factor,

as a function of (i) quantities easily measurable on site, like the discharge and the contaminant concentration in the monitoring well; (ii) hydraulic head in the well, in the polluted area and in the aquifer; (iii) the thickness of the cutoff wall; (iv) the spacing and the diameter of the wells. The evolution of such field scale values might help practitioners and agencies in recognizing a detrimental impact, that may require additional remedial actions to preserve the barriers functionality.

7 Acknowledgements

The study is part of the public administration agreement between Politecnico di Milano, Department of Civil and Environmental Engineering, and the Italian Ministry of Economic Development, Direzione Generale per la Sicurezza anche Ambientale delle Attività Minerarie ed Energetiche, Ufficio Nazionale Minerario per gli Idrocarburi e le Georisorse, Programme Clypea

References

Barvenik, M. J. and Ayres, J. E. (1987), 'Construction quality control and post-construction performance verification for the gilson road hazardous wales site cutoff wall', *NTIS, Springfield, VA(USA)* .

Bear, J. (2013), *Dynamics of fluids in porous media*, Courier Corporation.

Brenner, H. (1961), 'The slow motion of a sphere through a viscous fluid towards a plane surface', *Chemical Engineering Science* **16**(3-4), 242–251.

Britton, J. P., Filz, G. M. and Little, J. C. (2005), 'The effect of variability in hydraulic conductivity on contaminant transport through soil–bentonite cutoff walls', *Journal of Geotechnical and Geoenvironmental Engineering* **131**(8), 951–957.

Cermak, J., Evans, J. and Tamaro, G. J. (2012), Evaluation of soil-sement-bentonite wall performance-effects of backfill shrinkage, *in* 'Grouting and Deep Mixing 2012', pp. 502–511.

Della Vecchia, G. and Musso, G. (2016), 'Some remarks on single-and double-porosity modeling of coupled chemo-hydro-mechanical processes in clays', *Soils and Foundations* **56**(5), 779–789.

Du, Y.-J., Fan, R.-D., Reddy, K. R., Liu, S.-Y. and Yang, Y.-L. (2015), 'Impacts of presence of lead contamination in clayey soil–calcium bentonite cutoff wall backfills', *Applied Clay Science* **108**, 111–122.

Evans, J. C. (1993), Vertical cutoff walls, *in* 'Geotechnical practice for waste disposal', Springer, pp. 430–454.

Evans, J. C. (1994), Hydraulic conductivity of vertical cutoff walls, *in* 'Hydraulic conductivity and waste contaminant transport in soil', ASTM International.

Evans, J., Ororbia, M., Gutelius, J., Ruffing, D., Barlow, L. and Malusis, M. (2017), Soil-bentonite slurry trench cutoff wall lateral deformations, consolidation, stress transfer and hydraulic conductivity, *in* 'Proceedings of the 2nd symposium on coupled phenomena in environmental geotechnics (CPEG2), Leeds, UK', pp. 1–6.

Filz, G. M., Henry, L. B., Heslin, G. M. and Davidson, R. R. (2001), 'Determining hydraulic conductivity of soil-bentonite using the api filter press', *Geotechnical Testing Journal* **24**(1), 61–71.

Fratalocchi, E., Pasqualini, E. and Balboni, P. (2006), Performance of a cement-bentonite cut-off wall in an acidic sulphate environment, *in* '5th ICEG Environmental Geotechnics: Opportunities, Challenges and Responsibilities for Environmental Geotechnics: Proceedings of the ISSMGE's fifth international congress organized by the Geoenvironmental Research Centre, Cardiff University and held at Cardiff City Hall on 26–30th June 2006', Thomas Telford Publishing, pp. 133–139.

Grisolia, M. and Napoleoni, Q. (1997), Esempio di controllo di qualità di un diaframma plastico a protezione di una discarica di rifiuti, *in* 'Proceedings of the Simposio Internazionale di Ingegneria Sanitaria ed Ambientale SIDISA, Ravello (I), June', pp. 620–627.

Institution of Civil Engineers, I. (1999), 'Specification for the construction of slurry trench cut-off walls as barriers to pollution migration'.

Jefferis, S. (1981), Bentonite-cement slurries for hydraulic cut-offs, *in* 'Proceedings, Tenth In-

ternational Conference on Soil Mechanics and Foundation Engineering, Stockholm, Sweden', Vol. 1, pp. 435–440.

Jefferis, S. (2012), Cement-bentonite slurry systems, *in* 'Grouting and Deep Mixing 2012', pp. 1–24.

Joshi, K., Kechavarzi, C., Sutherland, K., Ng, M. Y. A., Soga, K. and Tedd, P. (2009), 'Laboratory and in situ tests for long-term hydraulic conductivity of a cement-bentonite cutoff wall', *Journal of Geotechnical and Geoenvironmental Engineering* **136**(4), 562–572.

Li, Y.-C., Chen, G.-N., Chen, Y.-M. and Cleall, P. J. (2017), 'Design charts for contaminant transport through slurry trench cutoff walls', *Journal of Environmental Engineering* **143**(9), 06017005.

Malusis, M. A. and McKeehan, M. D. (2013), 'Chemical compatibility of model soil-bentonite backfill containing multiswellable bentonite', *Journal of Geotechnical and Geoenvironmental Engineering* **139**(2), 189–198.

Manassero, M. (1994), 'Hydraulic conductivity assessment of slurry wall using piezocone test', *Journal of Geotechnical Engineering* **120**(10), 1725–1746.

Manassero, M. and Shackelford, C. (1994), 'The role of diffusion in contaminant migration through soil barriers', *Rivista Italiana di Geotecnica* **1**, 94.

Neville, C. J. and Andrews, C. B. (2006), 'Containment criterion for contaminant isolation by cutoff walls', *Groundwater* **44**(5), 682–686.

Opdyke, S. M. and Evans, J. C. (2005), 'Slag-cement-bentonite slurry walls', *Journal of Geotechnical and Geoenvironmental Engineering* **131**(6), 673–681.

Prince, M. J., Maneval, J. E. and Evans, J. C. (2000), Analysis of boundary conditions for contaminant transport through adsorptive, low-permeability slurry trench cutoff walls, *in* 'Environmental Geotechnics', pp. 58–72.

Rabideau, A. and Khandelwal, A. (1998), 'Boundary conditions for modeling transport in vertical barriers', *Journal of Environmental Engineering* **124**(11), 1135–1139.

Rowe, R. (2005), 'Long-term performance of contaminant barrier systems', *Géotechnique* **55**(9), 631–678.

Rowe, R. K., Hrapovic, L. and Kosaric, N. (1995), 'Diffusion of chloride and dichloromethane through an hdpe geomembrane', *Geosynthetics International* **2**(3), 507–536.

Rumer, R. R. and Mitchell, J. K. (1995), Assessment of barrier containment technologies, *in* 'International Containment Technology Workshop, Baltimore, Maryland', Citeseer, pp. 355–394.

Ryan, C. R. (1985), Slurry cutoff walls: Applications in the control of hazardous wastes, *in* 'Hydraulic barriers in soil and rock', ASTM International.

Ryan, C. R. (1987), Vertical barriers in soil for pollution containment, *in* 'Geotechnical practice for waste disposal '87', ASCE, pp. 182–204.

Sanetti, G. (1998), 'Diaframmi plastici a base di cemento bentonite', *Suolo & Sottosuolo* pp. 51–55.

Sanetti, G. (2000), 'Diaframmi plastici: evoluzione e nuovi sistemi di controllo post-operam', *Quarry and Construction* pp. 105–109.

Sanetti, G. (2006), 'Monitoraggio del diaframma plastico', *Quarry and Construction* pp. 88–92.

Scelsi, G., Della Vecchia, G., di Prisco, C., Musso, G. and Sanetti, G. (2019), Optimization of the geometry of monitoring devices for contaminant detection in cement-bentonite cutoff walls, *in* 'National Conference of the Researchers of Geotechnical Engineering', Springer, pp. 555–564.

Shackelford, C. D. (1990), 'Transit-time design of earthen barriers', *Engineering Geology* **29**(1), 79–94.

Smith, J. A. and Jaffe, P. R. (1994), 'Benzene transport through landfill liners containing organophilic bentonite', *Journal of Environmental Engineering* **120**(6), 1559–1577.

Takai, A., Inui, T. and Katsumi, T. (2016), 'Evaluating the hydraulic barrier performance of soil-bentonite cutoff walls using the piezocone penetration test', *Soils and Foundations* **56**(2), 277–290.

Trivedi, D., Holmes, R. and Brown, D. (1992), 'Monitoring the in-situ performance of a cement/bentonite cut-off wall at a low level waste disposal site', *Cement and Concrete Research* **22**(2-3), 339–349.

Van Genuchten, M. T. and Parker, J. (1984), 'Boundary conditions for displacement experiments through short laboratory soil columns 1', *Soil Science Society of America Journal* **48**(4), 703–708.

Appendix 1: Curing effect

In this Appendix, the effects of the time evolution of cement-bentonite hydraulic conductivity due to curing are considered. Inspired from the experimental data presented by Fratalocchi *et al.* (2006), the time needed for the backfill material to achieve a stable asymptotic hydraulic conductivity can be estimated to be $\sim$ 300 days. According to this evidence, an empirical evolution law for hydraulic conductivity, calibrated on the experimental data of Fig.14 was implemented in the numerical simulations:

$$K(t) = K_f + K_0 t^{-\alpha} \tag{12}$$

where $K_0 = 10^{-5}$ m/s is the initial value of the hydraulic conductivity of the liquid slurry, $\alpha = 2.3$ describes the maturation velocity of the mixture and K_f is the asymptotic value of the hydraulic conductivity (equal to 10^{-9} m/s; 10^{-10} m/s; 10^{-11}m/s respectively for $K_1(t)$, $K_2(t)$ and $K_3(t)$ as shown in Fig.14). Fig.14b shows the breakthrough curves at the outlet of the barrier (having adopted material properties as reported in Tab. 1, boundary conditions as described in Fig.3, $D = 5\text{x}10^{-10}\text{m}^2/\text{s}$ and $R = 100$) by considering the time evolution of K (dashed lines), as well as the same simulation run considering a constant value of K, equal to the asymptotic one. In all the cases, simulating the curing process does not provide any appreciable difference in terms of model predictions: the curing time is in fact negligible with respect to the time of contaminant transport across the barrier ($\sim 10^2$ years for $K = 10^{-11}$m/s, ~ 5 years for $K = 10^{-8}$m/s).

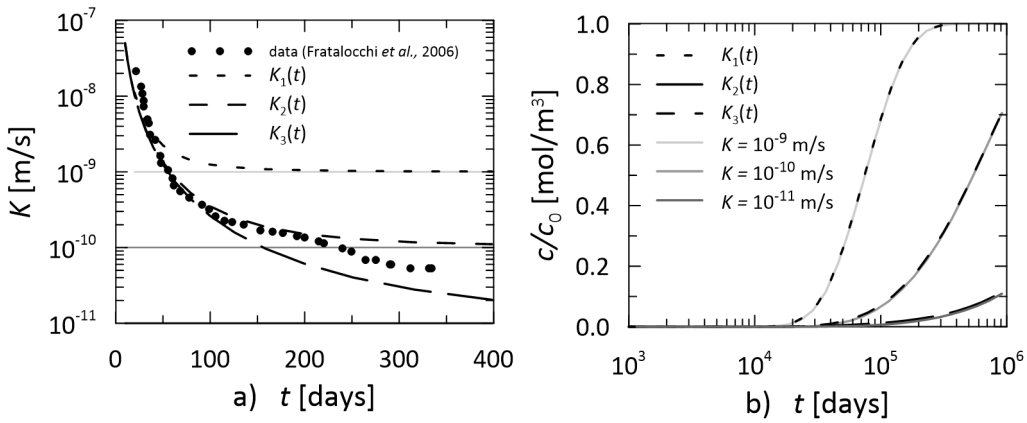

Figure 14: Effect of curing in cement bentonite mixtures: a) Evolution of hydraulic conductivity with time, b) breakthrough curves at the outlet of the barrier using different evolution laws for the hydraulic conductivity.

Appendix 2: Outlet boundary conditions

The choice of the boundary conditions to adopt for the solute mass balance equation was inspired by Brenner (1961) and Van Genuchten and Parker (1984), and are described in details on Section 3.3. However, Rabideau and Khandelwal (1998) also asserted that the most conservative boundary conditions to adopt for the solute transport through a cutoff wall are: a constant concentration BC at the inlet ($c(x = 0, t) = c_0$) and a zero concentration BC at the outlet ($c(x = l, t) = 0$), that maximize the concentration gradient between inlet and outlet, and inevitably induce a greater contaminant outflow flux. Assuming a Robin boundary condition at the inlet boundary, that ensures the conservation of mass contaminant, Figure 15 shows the results of simulations adopting a zero concentration gradient BC, compared to zero concentration BC at the outlet for the both hydraulic scenarios considered in the study. Figs 15a,b show the trends of the average value of the flux of contaminant across the outlet boundary with time: they are greater in the case of zero concentration BC, in accordance to what asserted by Rabideau and Khandelwal (1998). Figs 15c,d show the trend of the average contaminant concentration at the well boundary as a function of time. When a zero concentration BC is adopted at the outlet, the average value of contaminant concentration at the well boundary is as much mitigated as Pe is low. However, it is interesting to note that the first part of the trends, on which the method relies, for both the hydraulic scenarios and the Pe numbers, is not influenced by the type of outlet BC adopted. This leads to the univocal determination of the time t_0 and t_1 and of the slope θ of the trends (Eq.11), that are computed between $c_{dev}/c_0 = 1\% - 5\%$. Consequently the abaci presented in Figs. 9-12 are the same for both the type of outlet boundary conditions.

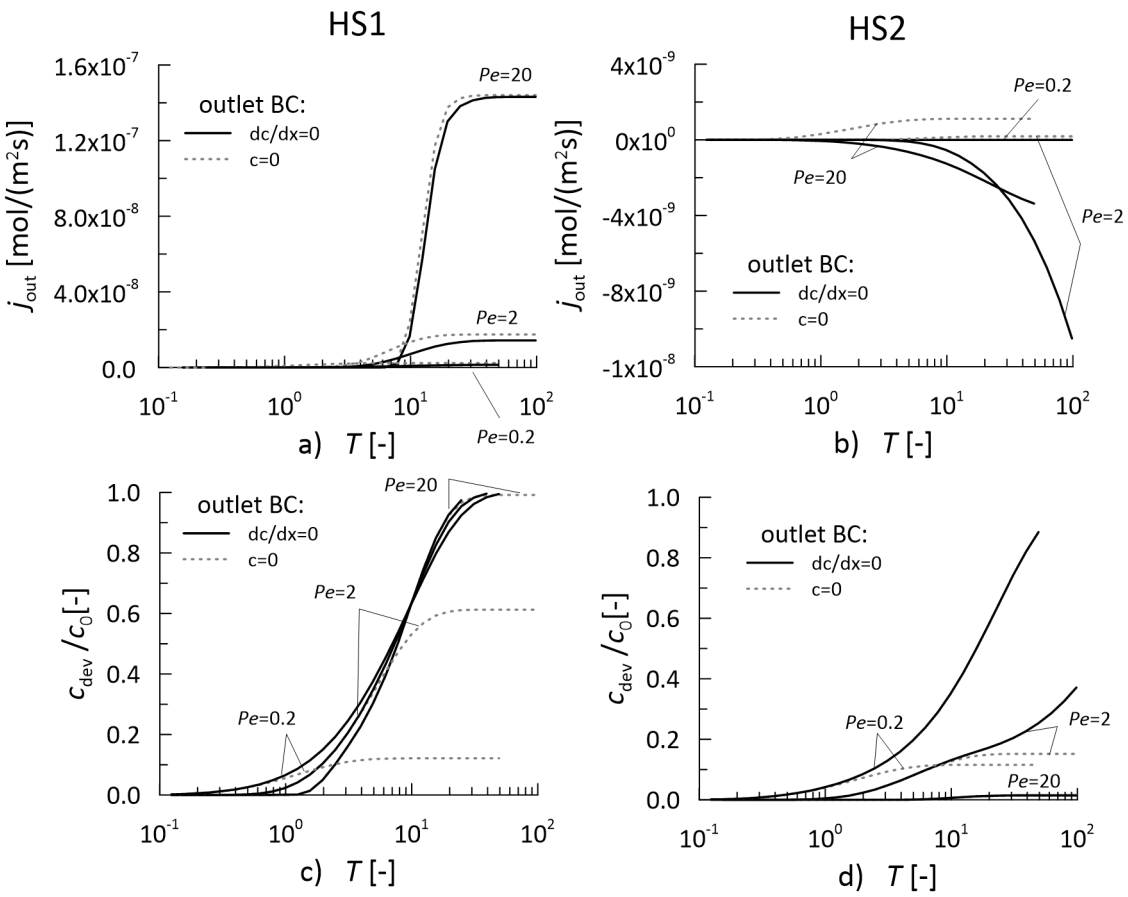

Figure 15: Comparisons results between zero gradient concentration and zero concentration boundary condition at the outlet. a,b) Trends of the average flux of contaminant along the outlet boundary for the hydraulic scenario a) 1 and b) 2; c,d) Trends of the average concentration of contaminant along the well boundary for the hydraulic scenario c) 1 and d) 2.